Stereolithography (SLA) 3D Printing of a Bladder Device for Intravesical Drug Delivery

Xiaoyan Xu[1], Alvaro Goyanes[1,2,3,*], Sarah J. Trenfield[1], Luis Diaz-Gomez[3], Carmen Alvarez-Lorenzo[3], Simon Gaisford[1,2] and Abdul W. Basit[1,2,*]

[1] Department of Pharmaceutics, UCL School of Pharmacy, University College London, 29-39 Brunswick Square, London, WC1N 1AX, UK

[2] FabRx Ltd., 3 Romney Road, Ashford, Kent TN24 0RW, UK

[3] Departamento de Farmacología, Farmacia y Tecnología Farmacéutica, I+D Farma (GI-1645), Facultad de Farmacia, and Health Research Institute of Santiago de Compostela (IDIS), Universidade de Santiago de Compostela, 15782 Santiago de Compostela, Spain

Abstract

Intravesical instillation therapy is an alternative approach to oral medications for the treatment of severe bladder diseases, offering high drug concentrations at the site of action while minimising systemic side effects. However, therapeutic efficacy is often limited because of the short residence time of the drug in the bladder and the need for repeated instillations. This study reports, for the first time, the use of stereolithography (SLA) 3D printing to manufacture novel indwelling bladder devices using an elastic polymer to achieve extended and localised delivery of lidocaine hydrochloride. The devices were designed to be inserted into and retrieved from the bladder using a urethral catheter. Two types of bladder devices (hollow and solid) were prepared with a resilient material (Elastic Resin) incorporating three drug loads of lidocaine hydrochloride (10% w/w, 30% w/w and 50% w/w); a drug frequently used to treat interstitial cystitis and bladder pain. All of the devices showed acceptable blood compatibility, good resistance to compressive and stretching forces and were able to recover their original shape immediately once external forces were removed. *In vitro* drug release studies showed that a complete release of lidocaine was achieved within 4 days from the hollow devices, whereas the solid devices enabled sustained drug release for up to 14 days. SLA 3D printing therefore provides a new manufacturing route to produce bladder-retentive drug delivery devices using elastic polymers, and offers a revolutionary and personalised approach for clinical intravesical drug delivery.

Keywords

Three-dimensional printing; Stereolithography; Additive manufacturing; Bladder; Intravesical drug delivery; Elastic polymers

1 Introduction

Severe bladder diseases, such as interstitial cystitis and bladder pain syndrome, affect millions of patients worldwide and have a significant impact on daily activities, social function and quality of life. Indeed, 7.9 million adult women in the United States alone have symptoms such as urinary urgency or frequency consistent with a possible diagnosis of interstitial cystitis or bladder pain syndrome [1]. Common therapies for bladder disorders are systemic (e.g. oral medications and transdermal patches), however these treatments often lead to undesirable side effects and limited efficacy at the disease site [2]. An alternative approach involves the intravesical instillation of drug-loaded solutions or suspensions directly into the bladder [3,4]. Favourably, intravesical installation enables localised high drug concentrations in the bladder, thereby improving treatment efficacy and reducing systemic exposure. However, the instilled drug solution or suspension can only be held by patients for a limited time (usually 20-60 min) and is voided by urination. For this reason, the drug residence time is limited and repeated treatments are required, leading to patient discomfort and non-adherence, as well as increasing the risk of infection [5,6].

Novel indwelling intravesical devices have recently been designed to be inserted and remain in the bladder in order to provide an extended drug release [7]. The devices are made from either biodegradable [8,9] or nonbiodegradable materials; the latter requiring removal via catheter after treatment. One nonbiodegradable example is the long-lasting intravesical pump technology called UROS™ (Situs Corporation Ltd.) [5], which involves a drug reservoir and a pressure-responsive valve to maintain a constant drug concentration over time. The device is inserted as a straight tube (10 cm length × 0.6 cm outer diameter), which transforms into a crescent shape when the drug solution is infused into it. UROS™ devices entered into clinical trials, however they did not progress beyond Phase II [10]. An alternative intravesical system, LiRIS™ (TARIS Biomedical)

was recently tested for lidocaine delivery and is currently in Phase II clinical trials [2]. The dual-lumen pretzel-shaped devices use a Nitinol wire to retain shape and provide retention, while drug is incorporated in the form of minitablets, enabling continuous drug release. Similarly, PharmaSphere (Innoventions Ltd.) is a floating system that contains an expandable balloon that is inflated in the bladder for sustained drug delivery [11,12]. Although these approaches are promising, the manufacturing processes of these devices are complex and require multiple steps, which makes them inherently time consuming and cost intensive.

Recently, three-dimensional (3D) printing has been explored as a potential disruptive technology to manufacture drug products and medical devices in the pharmaceutical and medical field [13,14]. 3D printing allows the fabrication of unconventional shapes with customised designs [15-18], tailored dosages [19-22], and drug release characteristics [23-26] that are impossible to make with traditional manufacturing methods, and thus allows a unique way to manufacture personalised drug products [27].

In the field of drug delivery, a number of different 3D printing technologies have been used, including extrusion-based, powder bed and vat photopolymerization techniques, all of which have been described elsewhere [28-35]. Among the different 3D printing technologies, vat photopolymerization techniques such as stereolithography (SLA) are especially appealing. The SLA printing process involves the production of solid objects by polymerization of liquid resins under light irradiation [36-38]. Compared with other 3D printing methods, SLA enables the precise production of devices with intricate geometries, superior feature resolution (as low as 25 microns) and a smooth surface finish. SLA printing offers two further advantages compared with extrusion-3D printing and laser sintering methods; objects are fabricated at room temperature, avoiding the risk of drug degradation (a characteristic which is particularly important for drug-loaded products and medical devices) and drugs can be incorporated into the resin prior to

printing either in solution or as a suspension, so aqueous solubility is not a factor in formulation development. To date, vat photopolymerization 3D printing has been explored to prepare innovative pharmaceutical formulations including oral dosage forms [39-41], hydrogels [42,43], multi-layer polypills [44], microneedles [45-48], implants [49-51], hearing aids [52,53] and dental devices [54-56], including the use of shape memory materials [57,58].

Elastic polymers (elastomers) are a class of materials that are capable of recovering their original shape following the removal of an external force (such as stretching or compression). Such polymers are characterised by having weak intermolecular forces, low Young's moduli and high failure strains compared with other materials. These characteristics are desirable for devices that require different conformations for insertion and for retention/drug release [59]; examples include self-expanding stents [60], vaginal rings [61] and gastric retentive devices [62,63]. Recently, fused deposition modelling (FDM) printing was proposed to prepare shape-changing drug delivery bladder devices using the polymer polyvinyl alcohol [64]. However, the selected model drug (caffeine) was not clinically relevant and its release was completed within 2 hours, which is likely too short for clinical intravesical drug delivery.

The aim of this study was to develop an elastomer-based bladder device with SLA 3D printing for intravesical drug delivery, specifically to combine the benefits of local bladder treatment with prolonged drug exposure. The device was designed to adopt a straight and rigid conformation to facilitate insertion and removal from the bladder via a urethral catheter, which would then undergo a shape change *in situ* to ensure retention in the bladder. Lidocaine hydrochloride was selected as the model compound because of its clinical relevance for treating bladder conditions such as interstitial cystitis or bladder pain syndrome. Two bladder device configurations (hollow and solid) were designed and

tested with three different drug loadings, and the solid-state characteristics, drug release and mechanical characteristics of the devices were assessed.

2 Materials and Methods

2.1 Materials

Lidocaine hydrochloride monohydrate (M_W 288.81 g/mol), magnesium chloride anhydrous ($MgCl_2$, ⩾98%) and urea (⩾99%) were obtained from Sigma-Aldrich (Dorset, UK). The printing polymer, Elastic Resin (a thermoset material), was purchased from Formlabs (USA). Gelucire® 48/16 was obtained from Gattefosse (Saint-Priest, Lyon, France). Potassium dihydrogen phosphate (KH_2PO_4, 99.5-100.5%), magnesium sulphate ($MgSO_4$, 99.7%), potassium chloride (KCl, 99.5-101.0%) and calcium chloride dihydrate ($Cacl_2 \cdot H_2O$, 99.0-103.0%) were acquired from VWR International Ltd. (Leicestershire, UK). Phosphoric acid (for HPLC, 85-90%) was purchased from Honeywell (Seelze, Germany). Sodium chloride (NaCl, ⩾99.5%) was obtained from Fisher Scientific (Loughborough, UK).

2.2 Design of the device

3D models of the devices were designed using 123D Design (Autodesk Inc., USA) with an S-shape, allowing their retention in the bladder (Figure 1). The designs could be elongated in a straight tube shape with a length of approximately 130 mm and an outer diameter of 3 mm, allowing insertion in the bladder with a urethral catheter. Two types of bladder device (hollow and solid) were designed. The hollow devices comprised a drug reservoir (0.5 mm shell thickness) and two holes (1 mm diameter) at the ends to allow loading of the drug as a melted solution into the devices and control the drug release. The solid devices were designed without any voids and were directly fabricated from the drug-loaded printing resin.

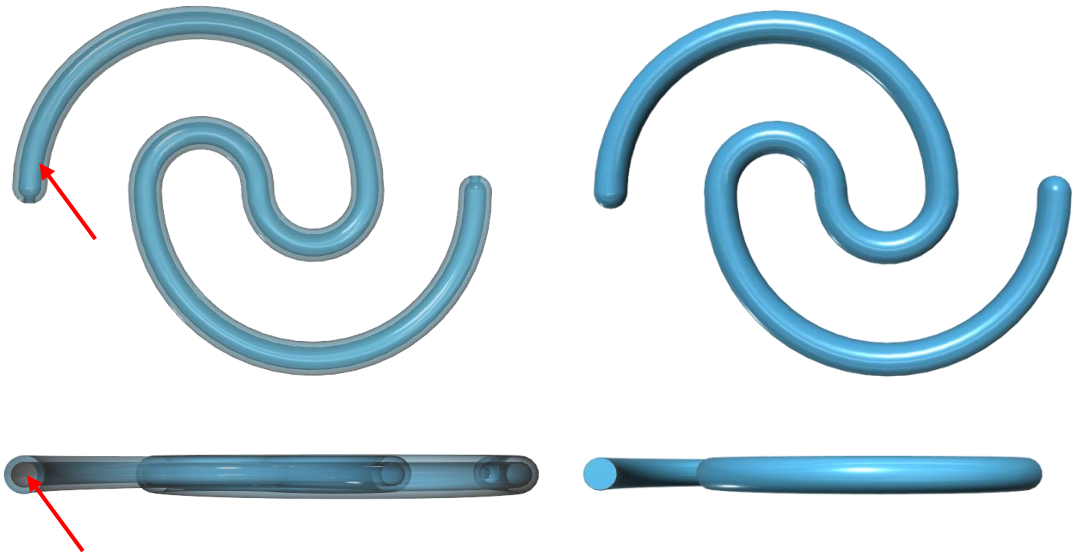

Figure 1. 3D Designs of the hollow (left) and solid (right) bladder devices (Arrows indicate the hollow space).

2.3 Preparation of drug-loaded photopolymer resins

The drug-loaded photopolymer resins were prepared by adding lidocaine hydrochloride into the Elastic Resin under stirring at room temperature (Table 1). The drug-loaded resins were directly loaded into the tray of the 3D printer. A control formulation (solid, with 0% drug load) was printed for X-ray micro computed tomography and mechanical testing comparison.

Table 1. Compositions (% w/w) of the drug-loaded photopolymer resins.

Formulations	Lidocaine (%)	Elastic Resin (%)
Solid 0% device	0	100
Solid 10% device	10	90
Solid 30% device	30	70
Solid 50% device	50	50

2.4 Printing process

A commercial Form 2 SLA 3D printer (Formlabs Inc., USA) equipped with a 405 nm laser was used to print the bladder devices. The 3D models of the devices were exported as a stereolithography (.stl) file to the Preform Software (Formlabs Inc., USA). The bladder devices were printed with supports on the build platform, selecting “Elastic” as the material setting, with a layer thickness of 50 µm. The SLA printed devices were washed with isopropyl alcohol (1 min for solid devices and 20 min for hollow devices) in Form Wash (Formlabs Inc., USA) to remove any uncured resin on the surface of the devices. Additionally, a post curing process was performed in a Form Cure (Formlabs Inc., USA) at 60°C for 20 min under a source of light (λ= 405 nm). All of the devices were used as printed after the removal of the supports using a side cutter.

2.5 Loading of the hollow devices

The filling of the hollow bladder device contained a mixture of different percentages of lidocaine hydrochloride and Gelucire® 48/16. Gelucire® 48/16 is a non-ionic water-dispersible surfactant with hydrophilic-lipophilic balance (HLB) values of 12, comprising polyethylene glycol (PEG) -32 (M_W 1500) mono- and diesters of palmitic (C_{16}) and stearic (C_{18}) acids and was chosen as a carrier due to its low melting point, water solubility and ease of manipulation for injection into the medical device [65]. The mixtures were prepared in a glass beaker by heating at 80°C under magnetic stirring to ensure complete dissolution of drug in the melted Gelucire® 48/16 (Table 2). The mixtures were then transferred to a 2 mL syringe (maintained at 80°C to avoid solidification) and were subsequently injected into the void cavity of the hollow bladder devices.

Table 2. Compositions (% w/w) of the drug-loaded formulations for the hollow devices.

Formulations	Lidocaine (%)	Gelucire (%)
Hollow 10% device	10	90
Hollow 30% device	30	70
Hollow 50% device	50	50

2.6 Thermal analysis

Differential scanning calorimetry (DSC) measurements were performed with a Q2000 DSC (TA instruments, Waters, LLC, USA) from 0 °C to 150 °C at a heating rate of 10 °C/min to characterise the gels and the drug loaded devices. Calibration for cell constant and enthalpy was performed as in a previous study [66]. TA aluminium pans and lids (Tzero) were used for each sample (8-10 mg) and a nitrogen purge of 50 mL/min was used for all the experiments. Data were collected with TA Advantage software for Q series (version 2.8.394) and analysed using TA Instruments Universal Analysis 2000. All melting temperatures are reported as extrapolated onset unless otherwise stated.

2.7 X-ray powder diffraction (XRPD)

Drug-loaded discs (23 mm diameter x 1 mm height) and discs without drugs (control) were printed with SLA. A Rigaku MiniFlex 600 (Rigaku, USA) equipped with a Cu Kα X-ray source (λ=1.5418Å) was used to obtain the XRPD patterns as in a previous study [66]. The intensity and voltage applied were 15 mA and 40 kV. Samples were scanned between 2θ = 3–60° with a stepwise size of 0.02° at a speed of 5°/min.

2.8 X-ray micro computed tomography (Micro-CT)

Small sections of the bladder devices were scanned using a high-resolution X-ray micro computed tomography (Micro-CT) scanner (SkyScan1172, Bruker-microCT, Kontich,

Belgium) with a resolution of 2000 × 1048 pixels to visualise the internal structures as in a previous study [67]. 3D imaging was performed by rotating the object through 360° with steps of 0.4° and four images were recorded for each of those. NRecon software (Version 1.7.0.4, Bruker-microCT) was used to reconstruct the images and the collected data were analysed using the software CT Analyzer (CTan version 1.16.4.1), where maps of different colours were used to represent the density of the devices.

2.9 Scanning electron microscopy (SEM)

Sections of the bladder device samples were attached to a self-adhesive carbon disc mounted on a 25 mm aluminium stub, which was coated with 25 nm of gold using a sputter coater. The stub was then placed into a FEI Quanta 200 FEG Scanning Electron Microscope (FEI, UK) at 5 kV accelerating voltage using secondary electron detection to obtain the cross-section images.

2.10 Determination of drug loading

For the solid bladder devices, drug loading was determined by cutting the devices into small pieces and dissolving them in 100 mL of isopropyl alcohol. In the case of the hollow bladder devices, the filling mixtures were dissolved in 100 mL of distilled water. Samples of solutions were filtered through 0.45 μm filters (Millipore Ltd., Ireland) and the concentration of drug was determined with HPLC (Hewlett Packard 1260 Series HPLC system, Agilent Technologies, Cheadle, UK). The stationary phase was an Eclipse plus C18 column, 100 mm × 4.6 mm (Zorbax, Agilent technologies, Cheshire, UK) and the mobile phase consisted of 0.01 M potassium dihydrogen phosphate (pH 2.1 adjusted with phosphoric acid) (80%) and acetonitrile (20%) at 30°C. The injection volume was 30 μL and the flow rate was kept at 1.0 mL/min. The eluent was screened at a wavelength of 214 nm and the retention time of lidocaine hydrochloride was at 3.5-3.6 min.

2.11 Dissolution testing conditions

Drug release from the SLA printed intravesical devices was determined using a shaking water bath (DMS360, Fisher Scientific, UK), maintained at a speed of 60 oscillations/min at $37 \pm 0.5℃$ (n=3). Drug-loaded devices were incubated in 500 mL of simulated urine fluid (composed of NaCl 13.75, $MgSO_4$ 1.69, $MgCl_2$, 0.83, $CaCl_2$ 0.67, KCl 0.38, and urea 17.40 g/mL, pH 7.50) [68] in glass bottles. 2 mL of fluid samples were withdrawn at predetermined time intervals and an equal volume of medium was replaced. The concentration of drug was determined using HPLC (as per the method in section 2.10).

The f_2 similarity factor developed by Moore and Flanner was used to compare the dissolution profiles of the devices with different drug loadings [69]. The similarity factor (f_2) is a logarithmic reciprocal square root transformation of the sum of the squared error and can be calculated using the equation (1)

$$f_2 = 50 \times log\left\{\left[1 + \frac{1}{n}\sum_{t=1}^{n}(R_t - T_t)^2\right]^{-\frac{1}{2}} \times 100\right\} \quad (1)$$

Where n is the number of dissolution time points, R_t and T_t are the percentage of drug released from the reference and test formulations at time point t, respectively [70]. The f_2 value ranges between 0 to 100 and a higher f_2 value indicates more similarity between the release profiles of the reference and test formulations [71].

2.12 Mechanical Tests

To determine the effect of lidocaine on the mechanical properties of the formulation, a tensile test was carried out using an Instron 5567 Universal Testing Machine at room temperature. The 3D model of the tensile bar was designed based on the guidelines from the American Society Testing Materials (ASTM) D638 type IV [72] at a scale of 50%

(Supplementary Figure A) and fabricated using the same printing process as in Section 2.4. The dimensions (length, width and thickness) of each tensile bar were measured using a digital calliper and recorded in the software. Following the guidelines from the ASTM standard D638-2014, the speed of testing was chosen as 50 mm/min for non-rigid specimens to give ruptures within 0.5 min to 5 min testing time. Five tensile bars were tested in each group and the failure at the narrow section of the tensile bar was expected. Compression testing was performed using the same Instron equipment with a 50 N load cell.

2.13 Haemolysis assessment

The haemolytic properties of the printed bladder devices were evaluated following the international standard ISO 10993-4:2017 for biological evaluation of medical devices. Whole blood was provided by the Galician transfusion center (ADOS) and obtained from anonymized healthy donors after obtaining written informed consent, in agreement with the Spanish legislation (Law 14/2007 on Biomedical Research). Samples of ca. 1 cm length (100 mg) were placed in 2 mL low adhesion microcentrifuge tubes. Additionally, to evaluate the haemolytic effect of the drug, NaCl 0.9% aqueous solutions of lidocaine (final concentrations of 50, 25, 12.5, 6.2 and 3.1 mg/mL, 100 µL per sample) were also tested. 1 mL of human whole blood previously diluted (1:30 v/v) in aqueous NaCl 0.9% was added to each sample and incubated for 60 min at 37 ºC and 100 rpm in an orbital shaker. Samples were centrifuged for 10 min at 10,000 rpm. Supernatants were immediately collected and 100 µL of each sample were placed individually in a 96 well plate and the absorbance at 540 nm was recorded using a plate reader (BIORAD Model 680 Microplate Reader, USA). A NaCl 0.9% aqueous solution and a 4% Triton X100 aqueous solution (100 µL per tube) were used as negative and positive controls, respectively. Finally, the percentage of haemolysis was calculated as follows (Equation 2):

$$Hemolysis\ (\%) = 100\ x\ \frac{(Abs_{sample} - Abs_{negative\ control})}{(Abs_{positive\ control} - Abs_{negative\ control})} \quad (2)$$

2.14 Statistical analysis

Drug dissolution tests and mechanical tests were performed in triplicate and sextuplicate, respectively. All numerical results were presented as mean ± standard deviation (SD), unless otherwise specified. Error bars represent standard deviation. Data from the mechanical tests were statistically analysed by performing one-way ANOVA with Tukey's post-hoc test executed (OriginPro 2017, OriginLab corporation, Northampton, MA, USA). $P < 0.05$ was considered statistically significant. Significance level notation was expressed as * for $p < 0.05$, ** for $p < 0.01$, *** for $p < 0.001$, and **** for $p < 0.0001$.

3 Results and discussion

Bladder devices were designed and manufactured using SLA printing to be implanted in the bladder via a catheter to provide sustained release of lidocaine for a predetermined period of time.

3.1 Hollow bladder devices

Hollow bladder devices were fabricated in two steps; first, SLA 3D printing was used to produce the shell of the device and, second, lidocaine-loaded Gelucire formulations were filled into the hollow device. Hollow 10%, 30%, and 50% bladder devices were successfully prepared (Figure 2, Top). All of the 3D printed bladder devices were fabricated similarly to the 3D model design with good consistency and a smooth surface finish. In general, the catheter size for adults range from 14 to 16 Fr (outer diameter 4.62 – 5.28 mm). The average outer diameter of the SLA printed hollow devices was 3.00 ± 0.02 mm, which was thin enough to be fitted into the catheter to be implanted into the

bladder. The average weight was 774.35 ± 20.41 mg. Approximately 254.40 ± 24.17 mg of a mixture of Gelucire and drug could be fitted into the hollow cavity, correlating to 25 mg, 75 mg, and 125 mg of lidocaine being loaded into the hollow 10%, 30%, and 50% devices. The devices were transparent before loading of the mixture of drug and excipient and showed an opaque and cream-coloured aspect after loading of the mixture. The flexibility of the hollow bladder devices was tested under external force (Figure 2, bottom). The devices could be stretched into a straight tube shape, and they recovered their original shape when no force was applied. This feature is crucial for the bladder devices to enable retention in the bladder without being expelled or causing harm to the bladder wall while releasing the drug. Intravesical devices without a retention frame have been reported to be voided from the bladder of rabbits [2].

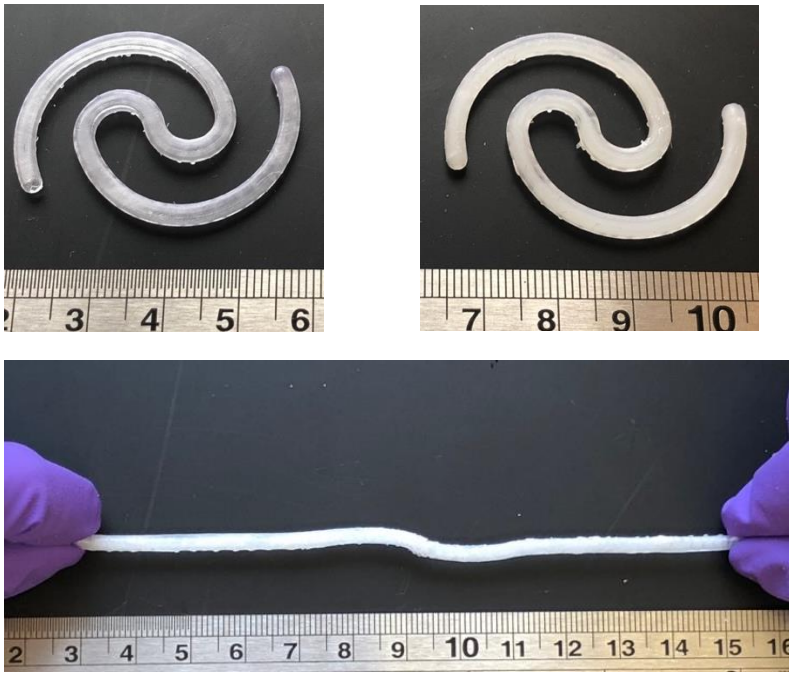

Figure 2. Photograph of a hollow bladder device before (top left) and after (top right) filling with 10% drug loading mixture; and the hollow 10% device under stretching (bottom). Scale in cm.

XRPD and DSC analyses were conducted to evaluate the physical state of the filling of the hollow bladder devices (Figure 3 (A) and (B)). The XRPD data showed that Gelucire exhibited partial crystallinity indicated by the two peaks at 19.1° and 23.4° 2θ. When the drug content increases, the intensity of the Gelucire peaks decrease. Similarly, the DSC results show that the sharp endothermic peak of the melting of lidocaine at 80°C was visible in the hollow 30% device and hollow 50% device, however no crystalline peaks of lidocaine (12.4°, 13.7°, 24.6°, and 25.5° 2θ) were observed by XRPD in any of the hollow formulations. This could be due to the fact that only a small portion of the drug remains in a crystalline form and not dissolved within the melted Gelucire carrier, and this is not observed using XRPD due to the lower sensitivity (>5%) of the method.

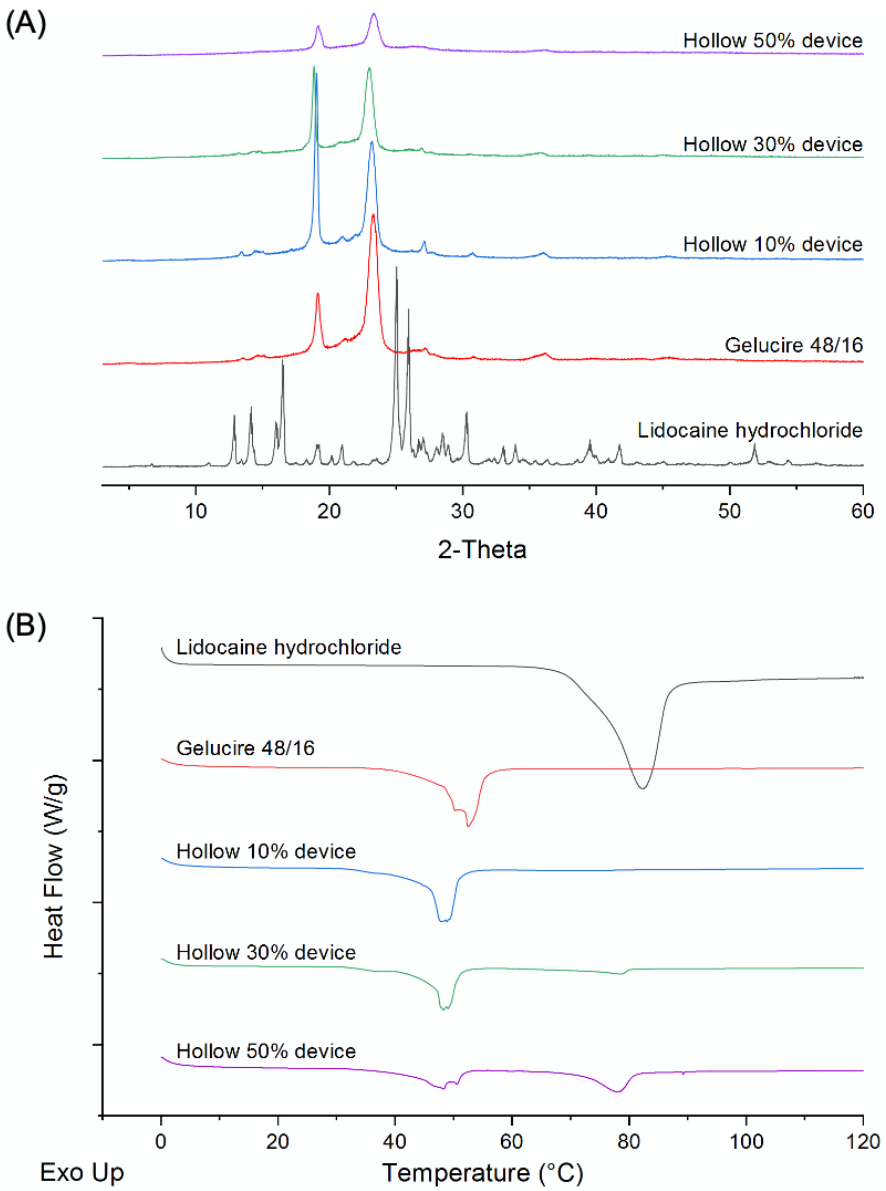

Figure 3. (A) X-ray powder diffractograms and (B) DSC thermograms of the pure drug and formulations with Gelucire.

X-ray micro-CT imaging was used to visualise the internal structure of the hollow bladder devices (Figure 4, Top). A clear distinction between the shell and the filling can be observed, indicating that the shell of the device was fabricated by SLA 3D printing with good resolution. The filling is mainly represented as a white colour in the images whereas the Elastic Resin has a red colour. By increasing the drug loading of lidocaine in the Gelucire formulations, an increased amount of white colour can be visualised, indicating

that the drug has a higher density compared with the Elastic Resin and Gelucire. The SEM images (Figure 4, Bottom) also confirmed that when the lidocaine loading increases, more drug particles are observed on the surface of the filling material.

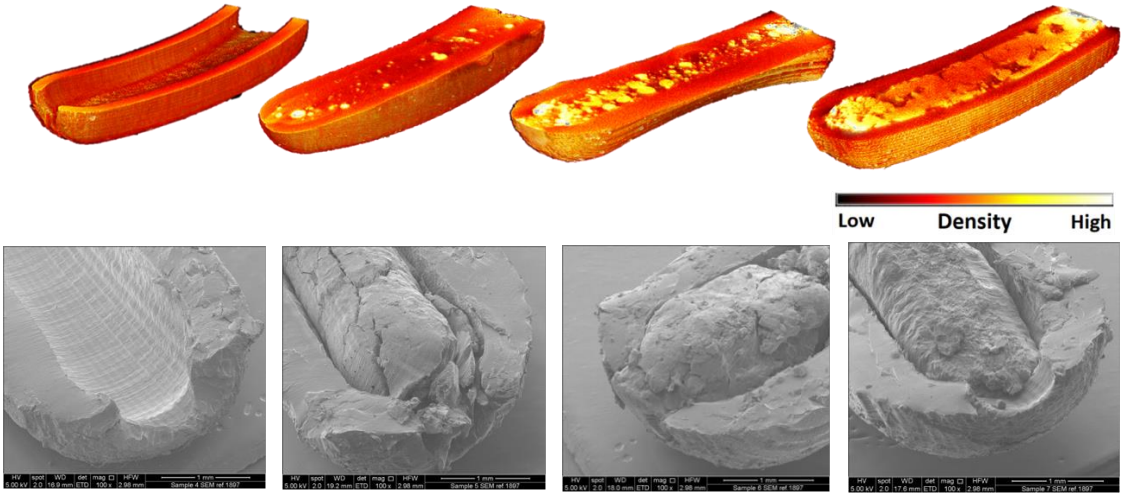

Figure 4. X-ray micro-CT images (top) and SEM images (bottom) of sections of the hollow bladder devices. From left to right, empty hollow device, hollow 10% device, hollow 30% device, and hollow 50% device. The scale bar in the micro-CT image is representative of density.

Drug loading of the filling material was evaluated before loading into the hollow bladder devices. The lidocaine contents for the hollow 10%, 30%, and 50% devices were 10.4% ± 0.6, 31.3% ± 0.9 and 48.7% ± 3.0, respectively, which are in agreement with theoretical drug loadings, confirming that no drug loss occurred during the preparation process. Drug dissolution profiles from the hollow bladder devices were obtained in 500 mL of simulated urine fluid to simulate the dissolution conditions in the bladder. Figure 5 shows the cumulative drug release profiles from the lidocaine-loaded hollow bladder devices over a 7-day period. Within the first 10 h, 46% lidocaine was released from the hollow 50% devices, whereas 31% and 19% were released from the hollow 30% and 10% devices, respectively. During the dissolution test, water entered into the hollow device through both holes on the sides of the devices and the mechanism of drug release was

through erosion of the Gelucire-lidocaine mixture. The increased drug release rate upon increased drug loading may be attributed to the drug having a higher solubility than the Gelucire. In the hollow 50% devices, all of the lidocaine was released in 3 days. For the hollow 10% and 30% devices, lidocaine was completely released after 4 days. The f_2 similarity factor revealed that the hollow 10% and 30% devices exhibited similar drug release profiles with a f_2 value of 63 (f_2 values between 50 and 100 indicate parity), whereas the lidocaine release from the hollow 50% devices showed significant differences in drug release rate from hollow 10% and 30% devices, (f_2 values of 42 and 47, respectively).

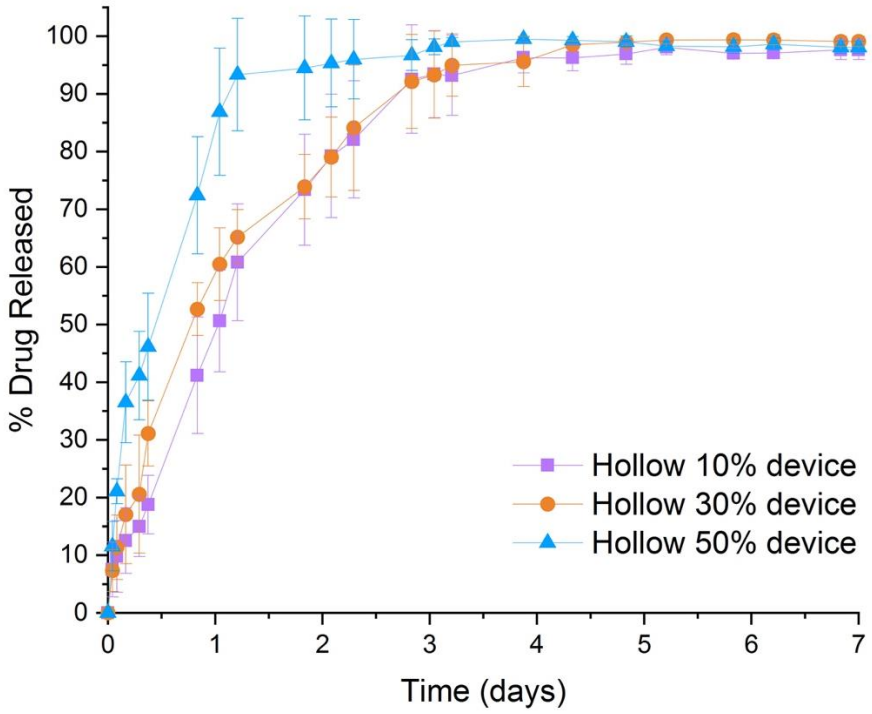

Figure 5. Cumulative release profiles of lidocaine hydrochloride from the SLA 3D printed hollow bladder devices. Data values represent mean ± SD (n=3).

The hollow bladder devices demonstrated prolonged lidocaine release over 4 days, which is an improvement in comparison to previously fabricated 3D printed drug loaded retentive devices, in which caffeine was completely released within 2 h [64]. It is worthy

to note, however, that whilst drug release over 4 days could improve the short-term compliance of patients with bladder pain syndrome or interstitial cystitis, a longer release profile would be more suitable for patients suffering from the condition chronically and reduce the need for the frequent invasive removal and insertions of devices.

3.2 Solid bladder devices

The solid bladder devices were designed to reduce the dissolution rate of lidocaine, increasing local drug exposure time. Prior to printing, when mixing the drug with the Elastic Resin, lidocaine was found as needle-shape crystals suspended in the resin and the number of crystals increased with the drug loading (Supplementary Figure B). Favourably, all of the solid devices were successfully printed, regardless of the drug loading (solid 10%, 30% and 50% devices) (Figure 6, Top) with average weights of 1411.7 ± 15.1 mg, 1564.7 ± 5.7 mg and 2549.2 ± 28.9 mg; corresponding with approximately 150 mg, 450 mg, and 1250 mg of lidocaine loaded in the solid 10%, 30%, and 50% devices, respectively. The outer diameters of the solid device were 3.10 ± 0.02 mm, 3.72 ± 0.06 mm, and 5.14 ± 0.17 mm, which were suitable for insertion via a catheter. In a similar manner to the hollow bladder device, the solid bladder device could withstand elongation and could instantaneously return to its initial design once the external force was removed (Figure 6, Bottom).

Figure 6. Photograph of the SLA 3D printed solid 10% device (top left), solid 30% device (top middle), and solid 50% device (top right) bladder devices and the solid 10% device under stretching (bottom). Scale in cm.

XRPD and DSC analyses were used to evaluate how the drug was incorporated into the devices. XRPD results showed the characteristic peaks of lidocaine hydrochloride at 16.6°, 25.0°, and 25.9° 2θ in the solid 10% device and solid 30% device, suggesting that lidocaine was present, to some extent, in the crystalline form (Figure 7 (A)). When the drug content was increased to 50%, almost all of the crystalline peaks of lidocaine hydrochloride were visible. The DSC thermograms (Figure 7 (B)) showed melting endotherms for lidocaine at 80°C in all the SLA printed formulations, again suggesting that the drug was present in the crystalline form. These results were consistent with light microscopy imaging, which showed the presence of drug crystals in the resin prior to the printing process (Supplementary File B).

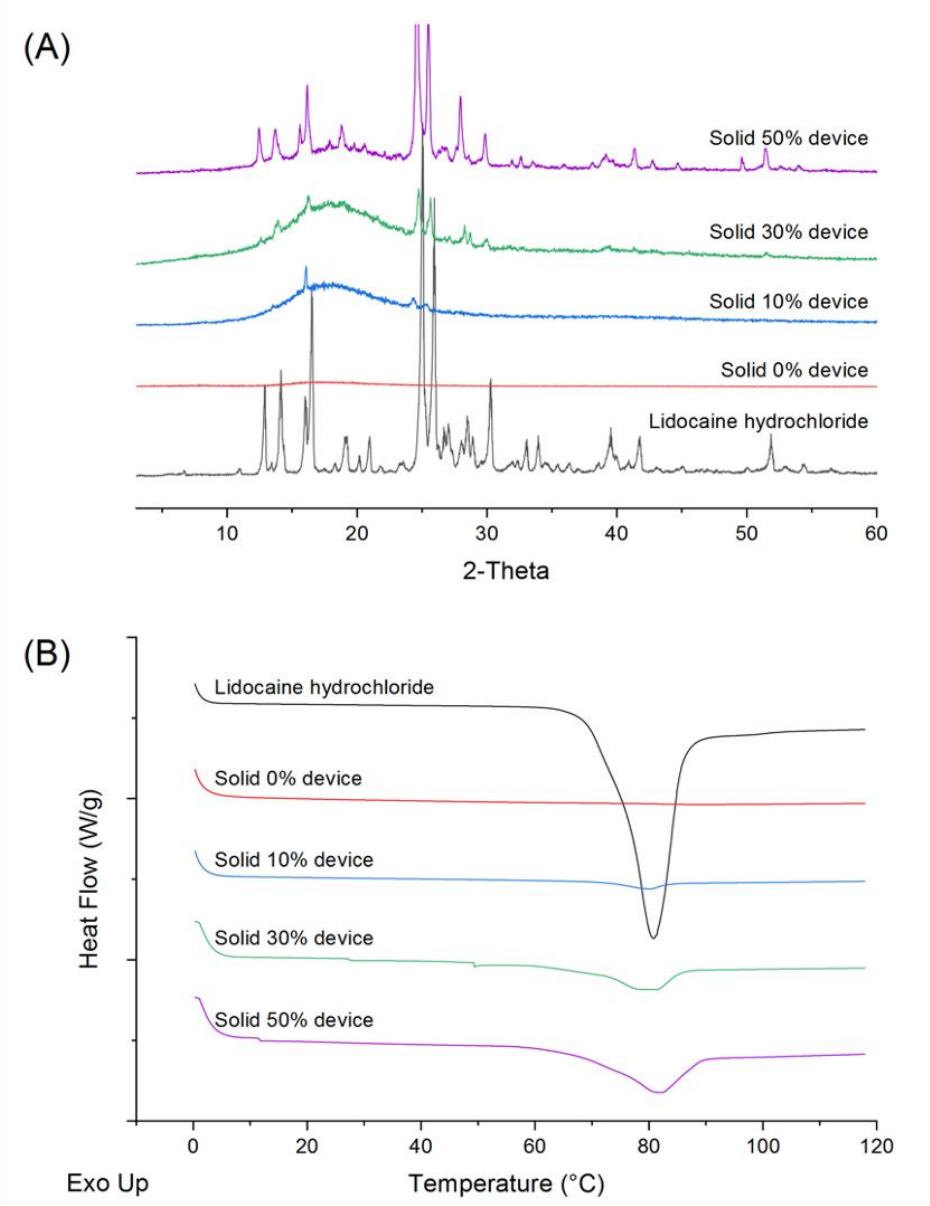

Figure 7. (A) X-ray powder diffractograms and (B) DSC thermograms of the pure drug and solid SLA 3D printed devices.

X-ray micro-CT imaging was employed to visualise the internal structures of the solid bladder devices (Figure 8, Top). Compared with the control solid device (fabricated without drug), lidocaine particles are clearly observed in the white colour; the number of white regions increased as a function of lidocaine concentration. Additionally, devices with higher drug loadings showed a lighter and brighter colour on the surface, due to the constructs having increased density. SEM images of the solid bladder devices (Figure 8,

Bottom) were consistent with the micro-CT results, with the surfaces of the 30% and 50% devices showing a rougher surface with an increased number of drug particles compared with the 0% and 10% devices that exhibited a smooth surface morphology.

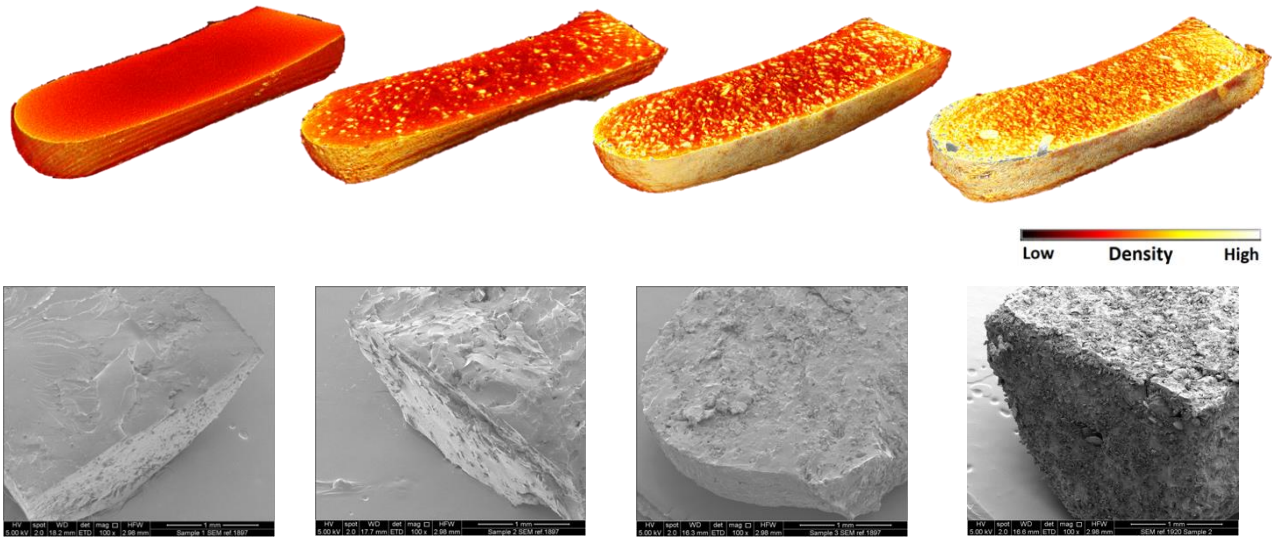

Figure 8. X-ray micro-CT images (top) and SEM images (bottom) of the sections of solid bladder devices. From left to right, solid 0% device, solid 10% device, solid 30% device, and solid 50% device. The scale bar in the micro-CT images is representative of density.

Mechanical properties of the solid bladder devices were evaluated by tensile mechanical testing using the standard dog-bone shaped tensile bars. Six tensile bars of the same thickness were printed for each formulation (Supplementary Figure C). The tensile stress-strain curves for each formulation are shown in Supplementary Figure D. It was observed that an increase in the relative concentration of Elastic Resin led not only to an increase in tensile stress but also an increase in elongation at break (Figure 9). Statistical analysis revealed that the groups showed significant differences between each other, with the exception of the tensile strength values of the solid 30% and 50% devices ($p > 0.05$). Compared with the tensile strength of the control (1.38 ± 0.07 MPa), the tensile strength of the solid 10% device was only slightly lower (1.19 ± 0.12 MPa) whereas for the solid 30% and 50% devices, the tensile strength values were significantly lower by

almost 30% (0.92 ± 0.02 and 0.89 ± 0.04 MPa respectively). On the other hand, the mean elongation at break of the control, solid 10%, solid 30%, and solid 50% devices were 102.70 ± 6.47%, 85.56 ± 5.29%, 69.36 ± 5.39%, and 58.05 ± 7.43%, respectively. A similar trend could be seen for tensile strength. This characteristic can be explained by the increased lidocaine content causing a reduction in the crosslinking density during printing, compromising the elasticity as well as the stiffness of the devices.

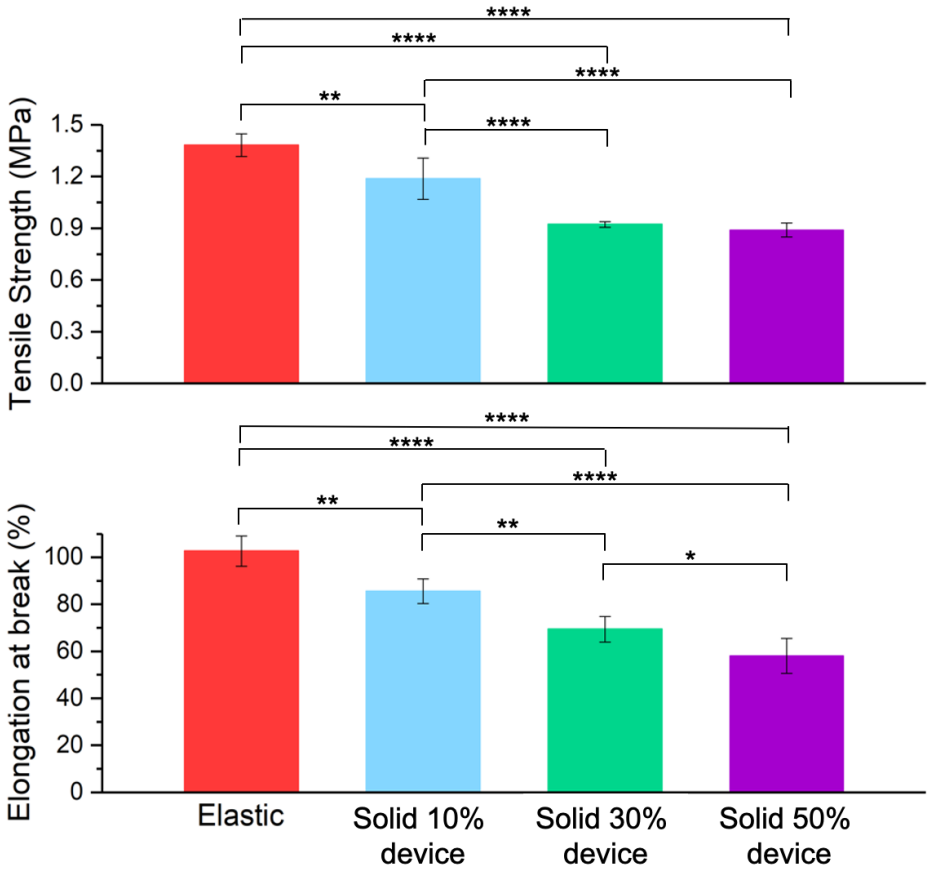

Figure 9. Mechanical properties of the SLA 3D printed tensile bars as a function of different drug loading of lidocaine. Columns and error bars represent means ± SD (n=6; * for $p < 0.05$, ** for $p < 0.01$, *** for $p < 0.001$, and **** for $p < 0.0001$).

The behaviour of the bladder devices under compressive force was also evaluated (Supplementary Figure E). All of the devices were strong enough to withhold the

compression force without breaking and, once the compressive load was removed, the devices were immediately able to recover to their original shape.

Drug loading of the devices was evaluated using HPLC. The lidocaine percentages of the solid 10%, solid 30% and solid 50% devices were 101.1% ± 6.9, 86.3% ± 3.3 and 97.7% ± 0.80, respectively. Drug release profiles for the solid bladder devices were obtained using the same conditions as for the hollow devices, but over a 14-day period (Figure 10). Initial 24h drug release of 17.8%, 28.8% and 74.1% were observed from the formulations solid 10%, solid 30% and solid 50% respectively. Decreasing the relative concentration of Elastic Resin was found to increase the drug release rate, because of a lower degree of crosslinking density in the polymeric matrix, enabling an accelerated diffusion of drug from the matrix. As expected, the devices with the highest percentage of lidocaine displayed the fastest release rate (90% of lidocaine was released in 3 days). Conversely, the solid 30% devices demonstrated first-order release kinetics across the 14 days, reaching 88% total release. The release profile from the solid 10% devices was almost linear, with approximately 3-4% lidocaine content released per day, reaching a total of 61% after 14 days. The f_2 similarity test showed that the drug dissolution profiles of the three formulations were significantly different, wherein f_2 values of 25, 16, and 33 were obtained for solid 10-30%, 10-50%, and 30-50% devices, respectively. The drug release from the solid bladder devices was comparable to the LiRIS devices where 66% and 62% of lidocaine was released from the 200 mg and 650 mg formulations after 14 days [10]. After the 14-day period, the solid devices were retrieved, dried and pictures were taken using SEM (Supplementary Figure F). Compared with the SEM images of the solid devices before the dissolution test, all of the devices exhibited porous surfaces, contributing to the release of lidocaine particles from the devices. An increased number of pores could be seen for devices with higher drug loading.

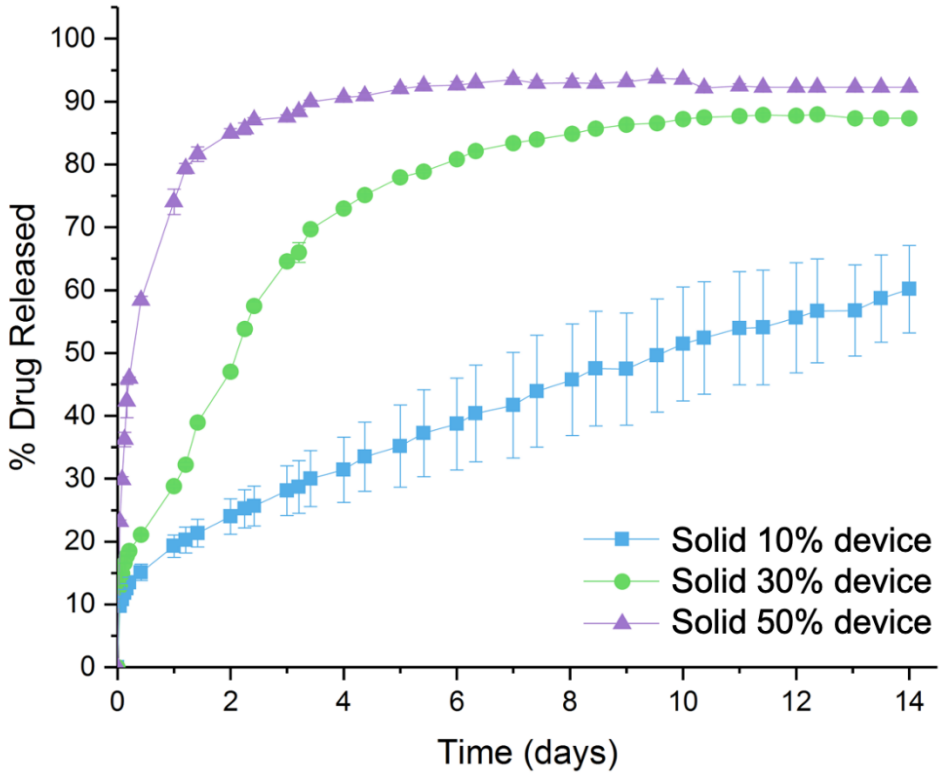

Figure 10. Cumulative release profile of lidocaine hydrochloride from the SLA 3D printed solid bladder devices. Data values represent mean ± SD, which are not seen in some data points as they are smaller than the symbols (n=3).

An alternative way of modifying the drug release profiles from the devices could be changing the selection of photoreactive resins. It has been previously reported that the selection of different types of resins modifies the drug release from drug-loaded hearing aids for patients suffering from ear infections *[52]*.

As an initial screening of the biocompatibility of the materials selected for the study, the haemolytic activity of the 3D printed devices was determined, since it is an essential criterion in the development of medical devices and implantable materials. The haemolytic activity of the solid 0% device was lower than 0.1%, a value similar to the negative control (Table 3). According to the international standard ISO 10993-4:2017, materials are considered as haemolytic if the haemolysis activity is higher than 5%. The

incorporation of 10% and 30% lidocaine in the medical devices resulted in haemolysis percentages of 2.2% (± 1.3) and 1.7% (± 3.5), respectively. The bladder device containing the highest concentration of lidocaine (solid 50% device) showed a haemolytic activity of 5.0% (± 1.5). The haemolytic effect of the free lidocaine aqueous solutions was tested to determine if the haemolytic activity of solid 50% devices could be due to the lidocaine content. Concentrations of lidocaine of 25 mg/mL and lower showed no haemolytic activity (haemolysis < 5%). However, the solutions containing lidocaine concentrations of 50 mg/mL led to an extensive haemolysis (16.0% ± 1.8). The results suggest that the developed medical devices containing up to 30% lidocaine are suitable for implantation in the human body without expecting haemolytic events, and that the haemolytic effect of the solid 50% device could be attributed to the drug.

Table 3. Haemolytic activity of the solid bladder devices and lidocaine solutions

Tested sample	Haemolysis (%)
Solid 0% device	0.1 ± 0.8
Solid 10% device	2.2 ± 1.3
Solid 30% device	1.7 ± 3.5
Solid 50% device	5.0 ± 1.5
Lidocaine 3.1 mg/mL	1.0 ± 1.3
Lidocaine 6.2 mg/mL	0.8 ± 1.4
Lidocaine 12.5 mg/mL	3.5 ± 1.0
Lidocaine 25 mg/mL	3.7 ± 0.9
Lidocaine 50 mg/mL	16.0 ± 1.8
Negative control (NaCl 0.9%)	0.0 ± 1.4
Positive control (4% Triton X100)	100.0 ± 5.5

The possibility of fabricating novel, implantable bladder drug delivery systems with 3D printing has been demonstrated. The use of two configurations (hollow and solid) were found to change the dissolution rates and profiles, and enabled the delivery of lidocaine for a prolonged period of time (2 weeks). The hollow and solid bladder devices both presented excellent retentive features and were capable of recovering their original S-shape conformation automatically and immediately; this compares favourably with the shape memory behaviour of the previously manufactured devices [64], which required body temperature (37°C) and water contact to achieve conformational changes. The bladder devices could also provide a versatile platform for the inclusion of other therapeutic agents for the treatment of other bladder disorders. Such a concept would be beneficial for increasing the drug indwelling time in the bladder and overcoming the discomfort of repeated instillations through catheters. In addition, devices could be prepared covering a wide range of sizes by scaling the dimensions of the 3D design (Supplementary Figure G) to provide personalised therapies to individual patients, highlighting the flexibility and reproducibility of the SLA 3D printing technology in producing drug delivery devices.

This study highlights the potential of SLA 3D printing to fabricate bladder devices using an easy and cost effective approach even when compared with alternative 3D printing methods, such as fused deposition modelling (FDM), which requires the preparation of drug-loaded filaments via hot melt extrusion that may cause thermal degradation of the drug *[73]*. Compared with the hollow devices, where drug release could be maintained over 4 days, the solid devices provided prolonged drug exposure for up to 14 days, beneficial for improving patient compliance. Devices containing a range of lidocaine dosages were successfully produced, which demonstrated differing drug release profiles, highlighting that SLA 3D printing is a highly flexible process, allowing easy modification of dosages to facilitate personalisation; particularly beneficial during early drug development whereby smaller bladder devices with a tailored dose could be easily

designed and manufactured to suit an animal study *[35,74]*. Favourably, the Elastic Resin used here is an elastic polymer, which is lighter, cheaper, easier to process, exhibits a higher extent of elastic deformation and excellent biocompatibility and potential biodegradability compared to the shape memory alloy used for LiRIS (Nitinol) *[75-77]*. This study highlights the potential of using innovative SLA 3D printing technologies for the manufacture of personalised and retentive drug delivery devices.

4 Conclusion

For the first time, novel indwelling intravesical devices have been developed using SLA 3D printing, providing sustained and localised lidocaine delivery to the bladder. Two types of bladder devices (hollow and solid) were successfully prepared using elastic polymers with different lidocaine content (10%, 30% and 50%). The printed devices exhibited excellent flexibility under stretching and compression and could immediately recover their original shape. Mechanical tests revealed that increasing lidocaine content decreased the strength and elongation at break of the tensile bars. Haemolysis tests demonstrated that the solid devices containing up to 30% of lidocaine exhibit good blood compatibility. *In vitro* drug release studies showed that the hollow devices enabled a complete release of lidocaine within 4 days, compared with up to 2 weeks for the solid devices. These proof-of-concept bladder devices showed drug release profiles comparable to other retentive intravesical devices found in the literature, yet the manufacturing process was simpler, more personalised and cost effective. This research presents a new opportunity for SLA 3D printing in the manufacture of implantable bladder drug delivery systems, allowing for a controlled delivery of lidocaine at the local site to avoid systemic side effects and improve patient compliance. By changing the selected drug, these devices could be easily adapted for the treatment of other bladder disorders, including overactive bladder disorder and bladder cancers, revolutionising intravesical treatment outcomes for patients.

Acknowledgement

This research was funded by the Engineering and Physical Sciences Research Council (EPSRC) UK, grant number EP/L01646X.

References

1. Berry, S.H.; Elliott, M.N.; Suttorp, M.; Bogart, L.M.; Stoto, M.A.; Eggers, P.; Nyberg, L.; Clemens, J.Q. Prevalence of symptoms of bladder pain syndrome/interstitial cystitis among adult females in the United States. *The Journal of urology* **2011**, *186*, 540-544.

2. Lee, H.; Cima, M.J. An intravesical device for the sustained delivery of lidocaine to the bladder. *Journal of Controlled Release* **2011**, *149*, 133-139.

3. Nickel, J.C.; Moldwin, R.; Lee, S.; Davis, E.L.; Henry, R.A.; Wyllie, M.G. Intravesical alkalinized lidocaine (PSD597) offers sustained relief from symptoms of interstitial cystitis and painful bladder syndrome. *BJU international* **2009**, *103*, 910-918.

4. Parsons, C.L. Successful downregulation of bladder sensory nerves with combination of heparin and alkalinized lidocaine in patients with interstitial cystitis. *Urology* **2005**, *65*, 45-48.

5. Fraser, M.O.; Lavelle, J.P.; Sacks, M.S.; Chancellor, M.B. The future of bladder control—intravesical drug delivery, a pinch of pepper, and gene therapy. *Reviews in Urology* **2002**, *4*, 1.

6. Lee, S.H.; Choy, Y.B. Implantable Devices for Sustained, Intravesical Drug Delivery. *International Neurourology Journal* **2016**, *20*, 101-106.

7. Zacchè, M.M.; Srikrishna, S.; Cardozo, L. Novel targeted bladder drug-delivery systems: a review. *Research and Reports in Urology* **2015**, *7*, 169.

8. Tobias, I.S.; Lee, H.; Engelmayr Jr, G.C.; Macaya, D.; Bettinger, C.J.; Cima, M.J. Zero-order controlled release of ciprofloxacin-HCl from a reservoir-based, bioresorbable and elastomeric device. *Journal of Controlled Release* **2010**, *146*, 356-362.

9. Von Walter, M.; Michaelis, I.; Jakse, G.; Grosse, J. Trospium chloride released from Intravesically applied PLGA-based carriers decreases bladder contractility in an insolated whole pig bladder model. *European Urology Supplements* **2009**, *8*, 178.

10. Nickel, J.C.; Jain, P.; Shore, N.; Anderson, J.; Giesing, D.; Lee, H.; Kim, G.; Daniel, K.; White, S.; Larrivee-Elkins, C. Continuous intravesical lidocaine treatment for interstitial cystitis/bladder pain syndrome: safety and efficacy of a new drug delivery device. *Science Translational Medicine* **2012**, *4*, 143ra100.

11. Innoventions Ltd. PharmaSphere Intravesical Drug Delivery. Availabe online:

https://www.innoventions-med.com/pharmasphere (accessed on 7th October).

12. Yachia, D.; Hirszowicz, E. Intravesicular balloon. US6293923B1, 2001.

13. Lim, S.H.; Kathuria, H.; Tan, J.J.Y.; Kang, L. 3D printed drug delivery and testing systems—a passing fad or the future? *Advanced drug delivery reviews* **2018**, *132*, 139-168.

14. Mohammed, A.; Elshaer, A.; Sareh, P.; Elsayed, M.; Hassanin, H. Additive manufacturing technologies for drug delivery applications. *International Journal of Pharmaceutics* **2020**, 119245.

15. Xu, X.; Zhao, J.; Wang, M.; Wang, L.; Yang, J. 3D Printed Polyvinyl Alcohol Tablets with Multiple Release Profiles. *Scientific reports* **2019**, *9*, 1-8.

16. Isreb, A.; Baj, K.; Wojsz, M.; Isreb, M.; Peak, M.; Alhnan, M.A. 3D printed oral theophylline doses with innovative 'radiator-like' design: Impact of polyethylene oxide (PEO) molecular weight. *International Journal of Pharmaceutics* **2019**, *564*, 98-105.

17. Sadia, M.; Arafat, B.; Ahmed, W.; Forbes, R.T.; Alhnan, M.A. Channelled tablets: An innovative approach to accelerating drug release from 3D printed tablets. *Journal of Controlled Release* **2018**, *269*, 355-363.

18. Awad, A.; Yao, A.; Trenfield, S.J.; Goyanes, A.; Gaisford, S.; Basit, A.W. 3D Printed Tablets (Printlets) with Braille and Moon Patterns for Visually Impaired Patients. *Pharmaceutics* **2020**, *12*, 172.

19. Goyanes, A.; Madla, C.M.; Umerji, A.; Piñeiro, G.D.; Montero, J.M.G.; Diaz, M.J.L.; Barcia, M.G.; Taherali, F.; Sánchez-Pintos, P.; Couce, M.-L. Automated therapy preparation of isoleucine formulations using 3D printing for the treatment of MSUD: First single-centre, prospective, crossover study in patients. *International Journal of Pharmaceutics* **2019**, *567*, 118497.

20. Smith, D.M.; Kapoor, Y.; Klinzing, G.R.; Procopio, A.T. Pharmaceutical 3D printing: Design and qualification of a single step print and fill capsule. *International Journal of Pharmaceutics* **2018**, *544*, 21-30.

21. Genina, N.; Boetker, J.P.; Colombo, S.; Harmankaya, N.; Rantanen, J.; Bohr, A. Anti-tuberculosis drug combination for controlled oral delivery using 3D printed compartmental dosage forms: From drug product design to in vivo testing. *Journal of Controlled Release* **2017**, *268*, 40-48.

22. Maroni, A.; Melocchi, A.; Parietti, F.; Foppoli, A.; Zema, L.; Gazzaniga, A. 3D printed multi-compartment capsular devices for two-pulse oral drug delivery.

Journal of Controlled Release **2017**, *268*, 10-18.

23. Gioumouxouzis, C.I.; Katsamenis, O.L.; Bouropoulos, N.; Fatouros, D.G. 3D printed oral solid dosage forms containing hydrochlorothiazide for controlled drug delivery. *Journal of Drug Delivery Science and Technology* **2017**, *40*, 164-171.

24. Goyanes, A.; Fina, F.; Martorana, A.; Sedough, D.; Gaisford, S.; Basit, A.W. Development of modified release 3D printed tablets (printlets) with pharmaceutical excipients using additive manufacturing. *International Journal of Pharmaceutics* **2017**, *527*, 21-30.

25. Sun, Y.; Soh, S. Printing Tablets with Fully Customizable Release Profiles for Personalized Medicine. *Advanced Materials* **2015**, *27*, 7847-7853.

26. Fina, F.; Goyanes, A.; Madla, C.M.; Awad, A.; Trenfield, S.J.; Kuek, J.M.; Patel, P.; Gaisford, S.; Basit, A.W. 3D printing of drug-loaded gyroid lattices using selective laser sintering. *International Journal of Pharmaceutics* **2018**, *547*, 44-52.

27. Basit, A.W.; Gaisford, S. *3D Printing of Pharmaceuticals*; Springer: 2018; Vol. 31.

28. Goole, J.; Amighi, K. 3D printing in pharmaceutics: A new tool for designing customized drug delivery systems. *International Journal of Pharmaceutics* **2016**, *499*, 376-394.

29. Alhnan, M.A.; Okwuosa, T.C.; Sadia, M.; Wan, K.W.; Ahmed, W.; Arafat, B. Emergence of 3D Printed Dosage Forms: Opportunities and Challenges. *Pharmaceutical Research* **2016**, *33*, 1817-1832.

30. Prasad, L.K.; Smyth, H. 3D Printing technologies for drug delivery: a review. *Drug development and industrial pharmacy* **2016**, *42*, 1019-1031.

31. Vithani, K.; Goyanes, A.; Jannin, V.; Basit, A.W.; Gaisford, S.; Boyd, B.J. An overview of 3D printing technologies for soft materials and potential opportunities for lipid-based drug delivery systems. *Pharmaceutical Research* **2019**, *36*, 4.

32. Akmal, J.S.; Salmi, M.; Mäkitie, A.; Björkstrand, R.; Partanen, J. Implementation of industrial additive manufacturing: intelligent implants and drug delivery systems. *Journal of functional biomaterials* **2018**, *9*, 41.

33. Gieseke, M.; Senz, V.; Vehse, M.; Fiedler, S.; Irsig, R.; Hustedt, M.; Sternberg, K.; Nölke, C.; Kaierle, S.; Wesling, V. Additive manufacturing of drug delivery systems. In Proceedings of 46th annual conference of the German Society for Biomedical Engineering (BMT 2012); pp. 425-442.

34. Awad, A.; Fina, F.; Goyanes, A.; Gaisford, S.; Basit, A.W. 3D printing: Principles and pharmaceutical applications of selective laser sintering. *International Journal of Pharmaceutics* **2020**, *586*, 119594.

35. Trenfield, S.J.; Awad, A.; Madla, C.M.; Hatton, G.B.; Firth, J.; Goyanes, A.; Gaisford, S.; Basit, A.W. Shaping the future: recent advances of 3D printing in drug delivery and healthcare. *Expert opinion on drug delivery* **2019**, 1081-1094.

36. Bagheri, A.; Jin, J. Photopolymerization in 3D Printing. *ACS Applied Polymer Materials* **2019**, *1*, 593-611.

37. Mendes-Felipe, C.; Oliveira, J.; Etxebarria, I.; Vilas-Vilela, J.L.; Lanceros-Mendez, S. State-of-the-art and future challenges of UV curable polymer-based smart materials for printing technologies. *Advanced Materials Technologies* **2019**, *4*, 1800618.

38. Xu, X.; Awad, A.; Martinez, P.R.; Gaisford, S.; Goyanes, A.; Basit, A.W. Vat photopolymerization 3D printing for advanced drug delivery and medical device applications. *Journal of Controlled Release* **2020**.

39. Healy, A.V.; Fuenmayor, E.; Doran, P.; Geever, L.M.; Higginbotham, C.L.; Lyons, J.G. Additive Manufacturing of Personalized Pharmaceutical Dosage Forms via Stereolithography. *Pharmaceutics* **2019**, *11*, 645.

40. Kadry, H.; Wadnap, S.; Xu, C.; Ahsan, F. Digital light processing (DLP) 3D-printing technology and photoreactive polymers in fabrication of modified-release tablets. *European Journal of Pharmaceutical Sciences* **2019**, *135*, 60-67.

41. Karakurt, I.; Aydoğdu, A.; Çıkrıkcı, S.; Orozco, J.; Lin, L. Stereolithography (SLA) 3D Printing of Ascorbic Acid Loaded Hydrogels: A Controlled Release Study. *International Journal of Pharmaceutics* **2020**, 119428.

42. Pawar, A.A.; Saada, G.; Cooperstein, I.; Larush, L.; Jackman, J.A.; Tabaei, S.R.; Cho, N.-J.; Magdassi, S. High-performance 3D printing of hydrogels by water-dispersible photoinitiator nanoparticles. *Science Advances* **2016**, *2*, e1501381.

43. Larush, L.; Kaner, I.; Fluksman, A.; Tamsut, A.; Pawar, A.A.; Lesnovski, P.; Benny, O.; Magdassi, S. 3D printing of responsive hydrogels for drug-delivery systems. *Journal of 3D printing in medicine* **2017**, *1*, 219-229.

44. Robles-Martinez, P.; Xu, X.; Trenfield, S.J.; Awad, A.; Goyanes, A.; Telford, R.; Basit, A.W.; Gaisford, S. 3D Printing of a Multi-Layered Polypill Containing Six Drugs Using a Novel Stereolithographic Method. *Pharmaceutics* **2019**, *11*, 274.

45. Johnson, A.R.; Caudill, C.L.; Tumbleston, J.R.; Bloomquist, C.J.; Moga, K.A.;

Ermoshkin, A.; Shirvanyants, D.; Mecham, S.J.; Luft, J.C.; DeSimone, J.M. Single-Step Fabrication of Computationally Designed Microneedles by Continuous Liquid Interface Production. *PLoS One* **2016**, *11*, e0162518.

46. Yao, W.; Li, D.; Zhao, Y.; Zhan, Z.; Jin, G.; Liang, H.; Yang, R. 3D Printed Multi-Functional Hydrogel Microneedles Based on High-Precision Digital Light Processing. *Micromachines* **2020**, *11*, 17.

47. Economidou, S.N.; Pere, C.P.P.; Reid, A.; Uddin, M.J.; Windmill, J.F.; Lamprou, D.A.; Douroumis, D. 3D printed microneedle patches using stereolithography (SLA) for intradermal insulin delivery. *Materials Science and Engineering: C* **2019**, *102*, 743-755.

48. Uddin, M.J.; Scoutaris, N.; Economidou, S.N.; Giraud, C.; Chowdhry, B.Z.; Donnelly, R.F.; Douroumis, D. 3D printed microneedles for anticancer therapy of skin tumours. *Materials Science and Engineering: C* **2020**, *107*, 110248.

49. Bloomquist, C.J.; Mecham, M.B.; Paradzinsky, M.D.; Janusziewicz, R.; Warner, S.B.; Luft, J.C.; Mecham, S.J.; Wang, A.Z.; DeSimone, J.M. Controlling release from 3D printed medical devices using CLIP and drug-loaded liquid resins. *Journal of Controlled Release* **2018**, *278*, 9-23.

50. Yang, Y.; Zhou, Y.; Lin, X.; Yang, Q.; Yang, G. Printability of External and Internal Structures Based on Digital Light Processing 3D Printing Technique. *Pharmaceutics* **2020**, *12*, 207.

51. Janusziewicz, R.; Mecham, S.J.; Olson, K.R.; Benhabbour, S.R. Design and Characterization of a Novel Series of Geometrically Complex Intravaginal Rings with Digital Light Synthesis. *Advanced Materials Technologies* **2020**, 2000261.

52. Vivero-Lopez, M.; Xu, X.; Muras, A.; Otero, A.; Concheiro, A.; Gaisford, S.; Basit, A.W.; Alvarez-Lorenzo, C.; Goyanes, A. Anti-biofilm multi drug-loaded 3D printed hearing aids. *Materials Science and Engineering: C* **2020**, 111606.

53. Banks, J. Adding value in additive manufacturing: researchers in the United Kingdom and Europe look to 3D printing for customization. *IEEE pulse* **2013**, *4*, 22-26.

54. Yue, J.; Zhao, P.; Gerasimov, J.Y.; van de Lagemaat, M.; Grotenhuis, A.; Rustema-Abbing, M.; van der Mei, H.C.; Busscher, H.J.; Herrmann, A.; Ren, Y. 3D-Printable antimicrobial composite resins. *Advanced Functional Materials* **2015**, *25*, 6756-6767.

55. Salmi, M.; Tuomi, J.; Sirkkanen, R.; Ingman, T.; Mäkitie, A. Rapid tooling method for soft customized removable oral appliances. *The open dentistry journal* **2012**,

6, 85.

56. Dawood, A.; Marti, B.M.; Sauret-Jackson, V.; Darwood, A. 3D printing in dentistry. *British dental journal* **2015**, *219*, 521-529.

57. Zarek, M.; Layani, M.; Cooperstein, I.; Sachyani, E.; Cohn, D.; Magdassi, S. 3D printing of shape memory polymers for flexible electronic devices. *Advanced Materials* **2016**, *28*, 4449-4454.

58. Zhao, Z.; Kuang, X.; Yuan, C.; Qi, H.J.; Fang, D. Hydrophilic/hydrophobic composite shape-shifting structures. *ACS applied materials & interfaces* **2018**, *10*, 19932-19939.

59. Lendlein, A.; Langer, R. Biodegradable, Elastic Shape-Memory Polymers for Potential Biomedical Applications. *Science* **2002**, *296*, 1673.

60. Chen, M.-C.; Tsai, H.-W.; Chang, Y.; Lai, W.-Y.; Mi, F.-L.; Liu, C.-T.; Wong, H.-S.; Sung, H.-W. Rapidly Self-Expandable Polymeric Stents with a Shape-Memory Property. *Biomacromolecules* **2007**, *8*, 2774-2780.

61. McCoy, C.F.; Apperley, D.C.; Variano, B.; Sussman, H.; Loeven, D.; Boyd, P.; Malcolm, R.K. Solid state 13C NMR spectroscopy provides direct evidence for reaction between ethinyl estradiol and a silicone elastomer vaginal ring drug delivery system. *International Journal of Pharmaceutics* **2018**, *548*, 689-697.

62. Bellinger, A.M.; Jafari, M.; Grant, T.M.; Zhang, S.; Slater, H.C.; Wenger, E.A.; Mo, S.; Lee, Y.-A.L.; Mazdiyasni, H.; Kogan, L. Oral, ultra–long-lasting drug delivery: application toward malaria elimination goals. *Science Translational Medicine* **2016**, *8*, 365ra157-365ra157.

63. Kirtane, A.R.; Abouzid, O.; Minahan, D.; Bensel, T.; Hill, A.L.; Selinger, C.; Bershteyn, A.; Craig, M.; Mo, S.S.; Mazdiyasni, H. Development of an oral once-weekly drug delivery system for HIV antiretroviral therapy. *Nature Communications* **2018**, *9*, 1-12.

64. Melocchi, A.; Inverardi, N.; Uboldi, M.; Baldi, F.; Maroni, A.; Pandini, S.; Briatico-Vangosa, F.; Zema, L.; Gazzaniga, A. Retentive device for intravesical drug delivery based on water-induced shape memory response of poly(vinyl alcohol): design concept and 4D printing feasibility. *International Journal of Pharmaceutics* **2019**, *559*, 299-311.

65. Gattefosse. Gelucire® 48/16. Availabe online: https://www.gattefosse.com/pharmaceuticals-products/gelucire-4816 (accessed on 7th October).

66. Xu, X.; Robles-Martinez, P.; Madla, C.M.; Joubert, F.; Goyanes, A.; Basit, A.W.; Gaisford, S. Stereolithography (SLA) 3D printing of an antihypertensive polyprintlet: Case study of an unexpected photopolymer-drug reaction. *Additive Manufacturing* **2020**, *33*, 101071.

67. Awad, A.; Fina, F.; Trenfield, S.J.; Patel, P.; Goyanes, A.; Gaisford, S.; Basit, A.W. 3D Printed Pellets (Miniprintlets): A Novel, Multi-Drug, Controlled Release Platform Technology. *Pharmaceutics* **2019**, *11*.

68. Sherif, A.Y.; Mahrous, G.M.; Alanazi, F.K. Novel in-situ gel for intravesical administration of ketorolac. *Saudi Pharmaceutical Journal* **2018**, *26*, 845-851.

69. Moore, J.W.; Flanner, H.H. Mathematical comparison of dissolution profiles. *Pharmaceutical technology* **1996**, *20*, 64-74.

70. Gohel, M.; Sarvaiya, K.; Shah, A.; Brahmbhatt, B. Mathematical approach for the assessment of similarity factor using a new scheme for calculating weight. *Indian journal of pharmaceutical sciences* **2009**, *71*, 142.

71. Shah, V.P.; Tsong, Y.; Sathe, P.; Liu, J.-P. In Vitro Dissolution Profile Comparison—Statistics and Analysis of the Similarity Factor, f2. *Pharmaceutical Research* **1998**, *15*, 889-896.

72. International, A. *ASTM D638-14, Standard Test Method for Tensile Properties of Plastics*; ASTM International: 2015.

73. Kollamaram, G.; Croker, D.M.; Walker, G.M.; Goyanes, A.; Basit, A.W.; Gaisford, S. Low temperature fused deposition modeling (FDM) 3D printing of thermolabile drugs. *International Journal of Pharmaceutics* **2018**, *545*, 144-152.

74. Goyanes, A.; Fernández-Ferreiro, A.; Majeed, A.; Gomez-Lado, N.; Awad, A.; Luaces-Rodríguez, A.; Gaisford, S.; Aguiar, P.; Basit, A.W. PET/CT imaging of 3D printed devices in the gastrointestinal tract of rodents. *International Journal of Pharmaceutics* **2018**, *536*, 158-164.

75. Liu, C.; Qin, H.; Mather, P. Review of progress in shape-memory polymers. *Journal of materials chemistry* **2007**, *17*, 1543-1558.

76. Jani, J.M.; Leary, M.; Subic, A.; Gibson, M.A. A review of shape memory alloy research, applications and opportunities. *Materials & Design (1980-2015)* **2014**, *56*, 1078-1113.

77. Sokolowski, W.; Metcalfe, A.; Hayashi, S.; Raymond, J. Medical applications of shape memory polymers. *Biomedical Materials* **2007**, *2*, S23.

Supplementary Material:

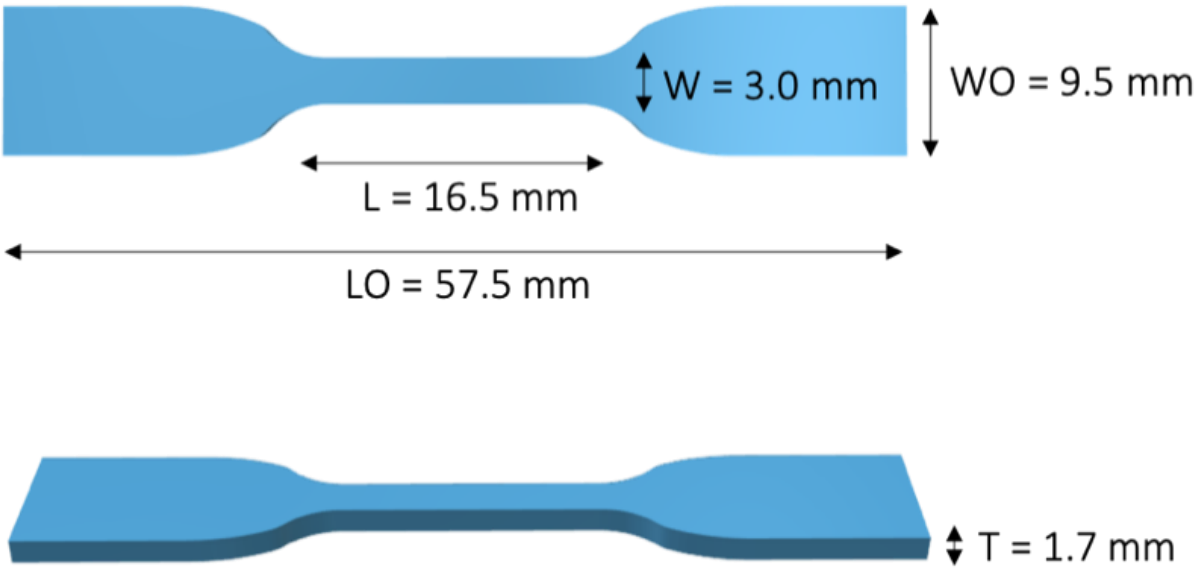

Supplementary Figure A. 3D model of the tensile bar.

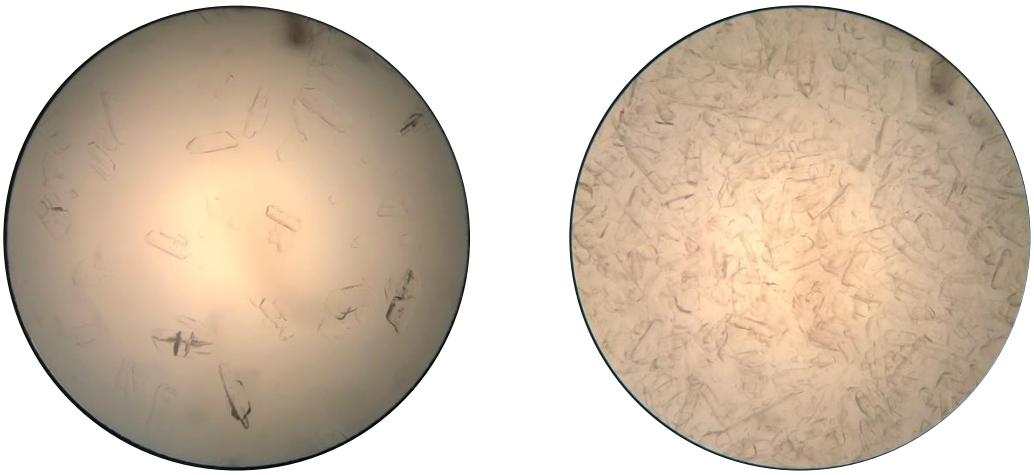

Supplementary Figure B. Formulations of (left) solid 10% device and (right) solid 30% device before SLA 3D printing under light microscope.

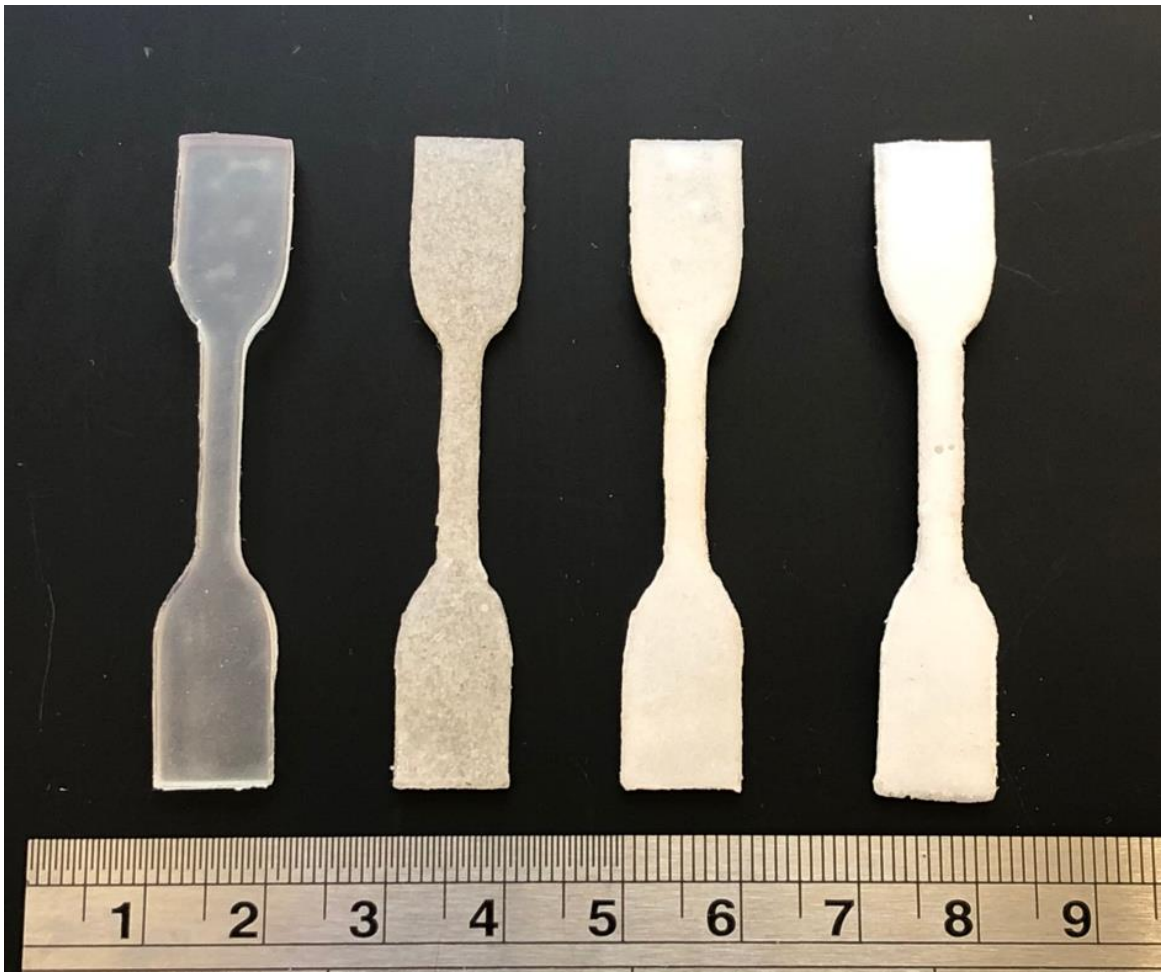

Supplementary Figure C. Photograph of the SLA 3D printed tensile bars printed with (from left to right), solid 0% device, solid 10% device, solid 30% device, and solid 50% device.

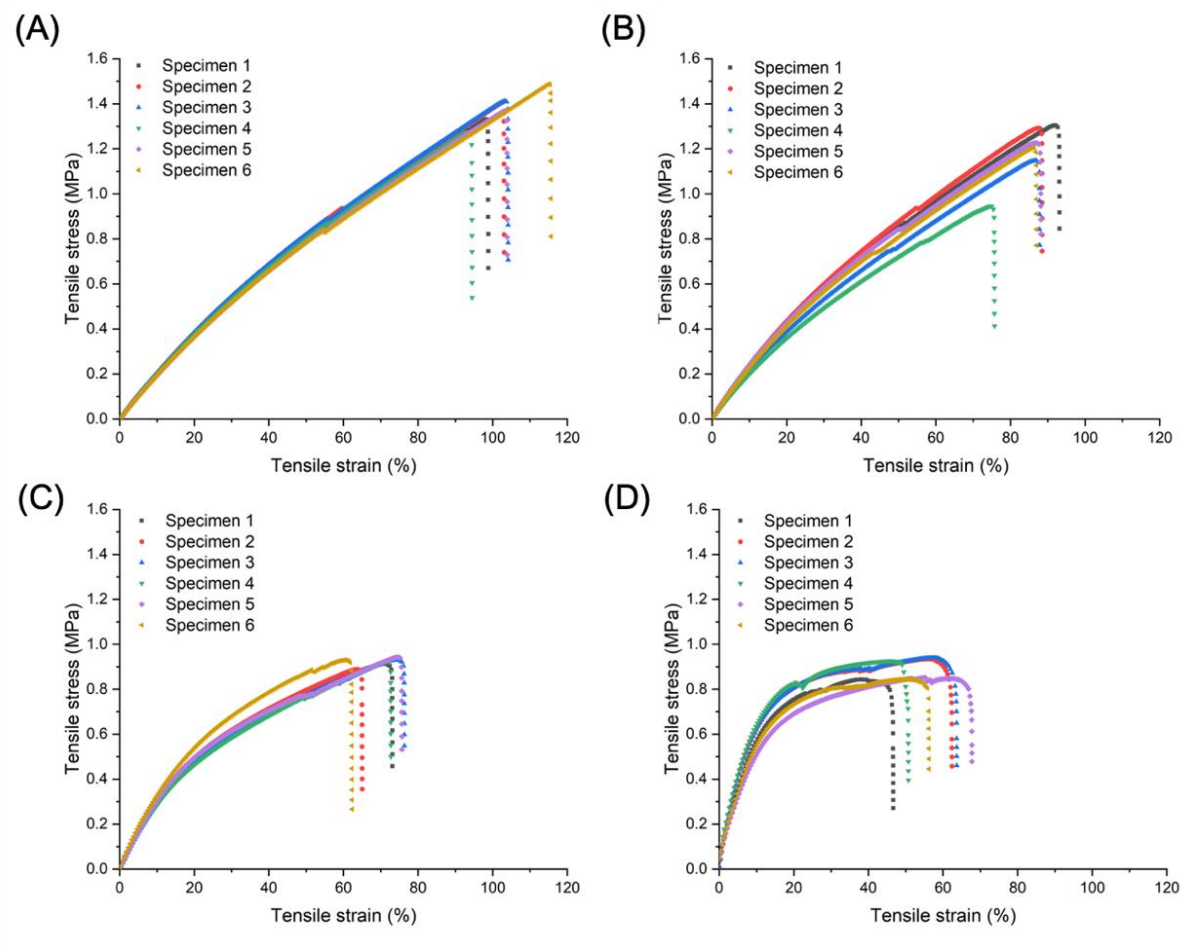

Supplementary Figure D. Stress-strain curves of the 3D printed (A) solid 0% loading, (B) solid 10% loading, (C) solid 30% loading, and (D) solid 50% loading tensile bars.

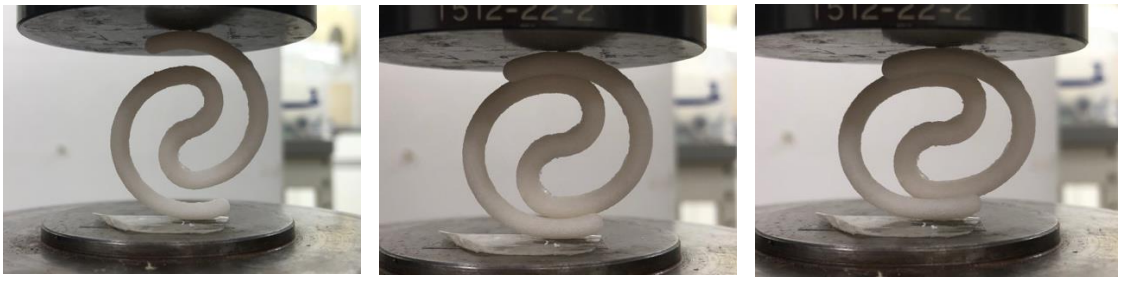

Supplementary Figure E. Behaviour of the solid 30% bladder device under compressive force.

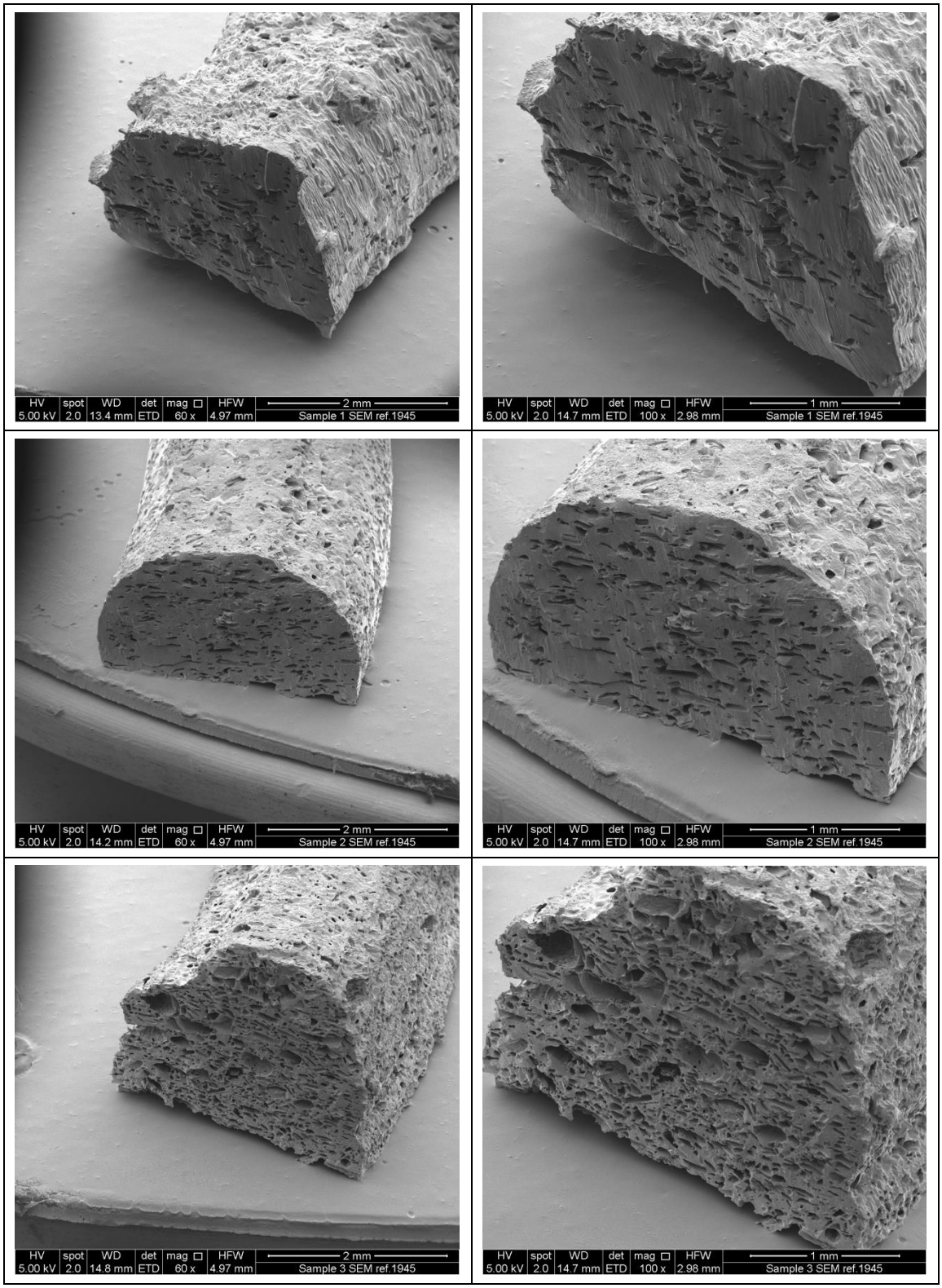

Supplementary Figure F. SEM images of sections of the solid bladder devices after dissolution studies. From top to bottom, solid 10% device, solid 30% device, and solid 50% device.

Supplementary Figure G. Photograph of the SLA 3D printed solid bladder devices in different sizes. From left to right, devices prepared with an scale factor of 0.5, 0.6, 0.7, 0.8, 0.9, and 1.0. Scale in cm.